Passive swimming in viscous oscillatory flows

Ikhee Jo, Yangyang Huang, Walter Zimmermann, and Eva Kanso

Passive swimming in viscous oscillatory flows

Ikhee Jo, Yangyang Huang, Walter Zimmermann, and Eva Kanso*

Electrical Engineering, University of Southern California, Los Angeles, CA, USA

Theoretische Physik I, Universität Bayreuth, D-95440 Bayreuth, Germany and

Aerospace and Mechanical Engineering,

University of Southern California, Los Angeles, CA, USA

(Dated: December 14, 2016)

Abstract

Fluid-based locomotion at low Reynolds number is subject to the constraints of Purcell's scallop theorem: reciprocal shape kinematics identical under a time-reversal symmetry cannot cause locomotion. In particular, a single degree-of-freedom scallop undergoing opening and closing motions cannot swim. Most strategies for symmetry-breaking and locomotion rely on direct control of the swimmer's shape kinematics. Less is known about indirect control via actuation of the fluid medium. To address how such indirect actuation strategies can lead to locomotion, we analyze a Λ-shaped model system analogous to Purcell's scallop but able to deform passively in oscillatory flows. Neutrally-buoyant scallops undergo no net locomotion. We show that *dense*, elastic scallops can exhibit passive locomotion in zero-mean oscillatory flows. We examine the efficiency of swimming parallel to the background flow and analyze the stability of these motions. We observe transitions from stable to unstable swimming, including ordered transitions from fluttering to chaotic-like motions and tumbling. Our results demonstrate that flow oscillations can be used to passively actuate and control the motion of microswimmers, which may be relevant to applications such as surgical robots and cell sorting and manipulation in microfluidic devices.

---

* kanso@usc.edu

I. INTRODUCTION

Biological and bioinspired swimmers move by shape actuation. The hydrodynamic forces acting on the swimmer are functions of the Reynolds number (Re). The Reynolds number measures the ratio of inertial to viscous effects. At low Re, viscous effects are dominant and fluid inertia is negligible. Locomotion in this regime is dominated by viscous drag forces and subject to the constraints of the scallop theorem [1]: reciprocal shape changes, that is to say, periodic shape changes identical under time reversibility, cannot display locomotion on average. Specifically, a scallop-like body with a single degree of freedom undergoing periodic opening and closing motions cannot move. To achieve a net displacement, microorganisms employ diverse propulsive strategies that break the time-reversal symmetry of viscous flows and circumvent the constraints of the scallop theorem. Examples include the helical movements of flagella [2–4] and the asymmetric beating patterns of cilia [5–7]. Minimal model systems that focus on the smallest level of complexity needed to generate a system capable of locomotion, such as Purcell's three-link swimmer [1, 8] and two- and three-sphere swimmers [9, 10], provide valuable insights into these symmetry-breaking mechanisms. These mechanisms rely mostly on direct shape actuation.

Less is known about locomotion by indirect actuation. Indirect actuation refers to leveraging the interactions between the fluid and body properties to achieve locomotion using partial or no direct control over the swimmer. To break the scallop theorem by indirect actuation, investigations focused on adding passive degrees of freedom to the swimmer [11, 12], considering the swimming problem in a viscoelastic fluid [13], adding inertia to the swimmer only while keeping the inertia of the fluid negligible [14], or adding a static separation between the centers of mass and buoyancy of the swimmer [15]. All these systems require partial control and actuation of the swimmer. The coupling between directly-actuated shape variables and passive body and fluid variables breaks the time reversal symmetry and leads to locomotion.

The important implications of breaking time reversibility, which enables the propulsion of microorganisms and microrobots in viscous flows, naturally compel one to ask whether there exist completely passive mechanisms for symmetry breaking and locomotion. More specifically, we ask whether by leveraging fluid-body interactions, we can achieve passive actuation of the swimmer via actuation of the fluid medium itself, such as via background

flow oscillations, with no direct control over the swimmer [16, 17]. Such actuation methods can be a key technology in various industrial and medical applications, including minimally-invasive surgery [18] and cell sorting and manipulation [19, 20]. Current microrobots utilize magnetic [21–24], electric [25, 26], chemical [27, 28], or optical [29] forces for actuation. Each of these actuation methods presents its own challenges, especially to medical applications, as they require external, often biologically incompatible, sources of power. Shape actuation in oscillatory flows via hydrodynamic forces only offers an attractive alternative for autonomous locomotion. In this study, we consider a minimal one degree-of-freedom system placed in oscillatory background flow with zero mean and show that locomotion is possible. This system is chosen for its obvious analogy to Purcell's scallop theorem and to provide physical insight into the symmetry-breaking mechanisms in oscillatory flows.

At low Re, the flow is governed by the linear Stokes equations, where drag forces depend linearly on the fluid velocity and cannot have non-zero mean in zero-mean oscillatory flows. In these oscillatory flows, a rigid body of the same density as the fluid and any shape moves back and forth with the flow and experiences zero net force over one oscillation period. A non-rigid body with one degree of freedom in oscillatory flows also experiences zero net displacement. Basically, rigid bodies and one degree-of-freedom deformable bodies, when placed in oscillatory flows of zero-mean velocity, undergo reciprocal motion and no net locomotion. We show that a one degree-of-freedom deformable body that is *denser* than the surrounding fluid is able to break the time reversible symmetry and propel itself forward in symmetric oscillatory flows. This symmetry-breaking mechanism is reminiscent but not identical to the one discussed in [14]. In the latter, examples of dense bodies subject to direct shape actuation and undergoing reciprocal motion are shown to swim in an otherwise quiescent fluid; here we demonstrate that dense bodies are able to swim *passively* in symmetric oscillatory flows. This motion is distinct from locomotion in oscillatory flows at finite Re, where propulsion is related to streaming flows and a fluid jet in the wake of the swimmer [30]. This motion in uniform oscillatory flows is also distinct from the migration of elastic bodies across streamlines in non-linear shear flows at zero Re [31–33].

We then examine the stability of passive swimming in oscillatory flows when the body is subject to rotational perturbations such that its axis of symmetry is no longer aligned with the direction of the background oscillatory flow. We find that for a range of parameter values, symmetric swimming is stable to perturbations. We closely examine the nonlinear behavior

in regions of the parameter space where symmetric swimming is unstable. We identify three types of behavior: fluttering, chaotic, and tumbling depending on the parameters of the swimmer and background flow. These results suggest that one can control the behavior of the swimmer by properly manipulating the parameters of the swimmer and background flow.

The organization of this paper is as follows: in section II, we derive the equations of motion for a two-link swimmer in oscillatory background flows. The behavior of the swimmer and its stability are illustrated in section III. The importance of these findings are discussed in section IV.

II. PROBLEM FORMULATION

a. Swimmer model. Our model swimmer consists of two slender bars, which we will refer to as arms, of equal length $\tilde{l}$ and density $\tilde{\rho}_s$, joined at the apex at an angle 2α via a massless torsional spring of stiffness $\tilde{\kappa}$; see Fig. 1. The mass of the arms is given by $\tilde{m} = \pi\tilde{a}^2\tilde{\rho}_s\tilde{l}$, where $\tilde{a}$ is the thickness of the arm and $\tilde{a}/\tilde{l} \ll 1$. The spring has a rest angle α_r. Deviations from α_r generate a torque $\tau = 2\tilde{\kappa}(\alpha - \alpha_r)$. The background fluid of density $\tilde{\rho}$ and viscosity $\tilde{\eta}$ oscillates linearly with velocity $\tilde{U} = \tilde{A}(\pi\tilde{f})\sin(2\pi\tilde{f}\tilde{t})$, where $\tilde{f}$ is the oscillation frequency and $\tilde{A}$ is the peak-to-peak oscillation amplitude and $\tilde{t}$ is time (in seconds).

b. Dimensionless parameters. We use $\tilde{l}$, $\tilde{T} = 1/\tilde{f}$ and $\tilde{\rho}$ as the length, time, and density scales, respectively. Non-dimensional analysis yields four independent, dimensionless parameters: the mass m and spring stiffness κ of the swimmer, and the amplitude A and viscosity η of the background flow,

$$m \triangleq \frac{\tilde{m}}{\tilde{\rho}\tilde{l}^3}, \quad \kappa \triangleq \frac{\tilde{\kappa}}{\tilde{\rho}\tilde{l}^4\tilde{f}^2}, \quad A \triangleq \frac{\tilde{A}}{\tilde{l}}, \quad \eta \triangleq \frac{\tilde{\eta}}{\tilde{\rho}\tilde{l}^2\tilde{f}}. \tag{1}$$

A few remarks on the order of magnitude of the dimensional and non-dimensional parameters are in order. For example, we consider a typical micro-swimmer of mass $\tilde{m} = 1\mu g$ ($\rho_s \approx 10^4 \mathrm{kg/m^3}$), spring stiffness $\tilde{\kappa} = 0.1(\mu g \cdot m)/s$ shouldn't this be $(\mu g \cdot m^2)/s^2$ and size $\tilde{l} = 100\mu m, \tilde{a} = 10\mu m$. Let the micro-swimmer be submerged in a fluid of density $\tilde{\rho} = 10^3 \mathrm{kg/m^3}$ and viscosity $\tilde{\eta} = 10^{-3}\mathrm{kg/(m \cdot s)}$ as in the case of water, with background flow oscillations of amplitude $\tilde{A} = 200\mu m$ and frequency $\tilde{f} = 1Hz$. Then the corresponding dimensionless

4

	mass	spring stiffness	flow amplitude	fluid viscosity
dimensional	$\tilde{m} = 1\mu\text{g}$	$\tilde{\kappa} = 0.1(\mu\text{g} \cdot \text{m})/\text{s}$	$\tilde{A} = 200\mu\text{m}$	$\tilde{\eta} = 10^{-3}\text{kg}/(\text{m} \cdot \text{s})$
dimensionless	$m = 1$	$\kappa = 1000$	$A = 2$	$\eta = 100$

TABLE I. One set of dimensional and non-dimensional parameters for the micro-swimmer in oscillatory flow.

parameters are $m = 1, \kappa = 1000, A = 2, \eta = 100$. See TABLE I.

More generally, two relevant Reynolds numbers can be used to characterize this system (see [14]): the fluid advective Reynolds number $\text{Re}_{\text{fluid}} = \tilde{\rho}\tilde{l}\tilde{A}\tilde{f}/\tilde{\eta}$; and the swimmer Reynolds number $\text{Re}_{\text{swimmer}} = \tilde{\rho}_s\tilde{l}^2\tilde{f}/\tilde{\eta}$. Here, we consider dense swimmers with $\tilde{A}/\tilde{l}$ be O(1) and $\tilde{\rho}_s/\tilde{\rho} \gg 1$ for which $\text{Re}_{\text{fluid}} \ll \text{Re}_{\text{swimmer}}$. That is, we consider the case of dense swimmers but negligible fluid inertia. For example, for the set of parameters in TABLE I, $\text{Re}_{\text{fluid}} = 0.02 < \text{Re}_{\text{swimmer}} = 0.1 < 1$. Note that this is equivalent to a small Stokes number $\text{Stk} = t_s/t_f$, defined as the ratio of the swimmer's relaxation time t_s in response to fluid drag forces to the fluid characteristic time $t_f = 1/\tilde{f}$. The non-dimensional mass $m = \pi\tilde{\rho}_s\tilde{a}^2/\tilde{\rho}\tilde{l}^2$ is O(1) given that we considered $\tilde{\rho}_s/\tilde{\rho} \gg 1$ and $\tilde{a}/\tilde{l} \ll 1$. We vary the stiffness κ over several orders of magnitude to explore its effect on the swimmer's behavior: small values of κ correspond to a 'floppy' swimmer while $\kappa \gg 1$ approaches a rigid swimmer. The dimensionless viscosity $\eta = A/\text{Re}_{\text{fluid}}$ must be large ($\eta \gg 1$) since $\text{Re}_{\text{fluid}} \ll 1$.

c. *Kinematics.* Let (x, y) denote the position of the apex of the swimmer in a fixed inertial frame $(\mathbf{e}_x, \mathbf{e}_y)$ where the x-direction is chosen to coincide with the direction of the background flow oscillations. Let θ denote the orientation of the swimmer from the x-axis. The translational and rotational velocities of the swimmer are given by $(\dot{x}, \dot{y})$ and $\dot{\theta}$. In addition, the opening angle α of the swimmer changes passively in time such that its rotational speed is denoted by $\dot{\alpha}$.

Consider an infinitesimal segment of the swimmer. The local translational velocity $\mathbf{u}$ at that segment due to the swimmer's translational and rotational motions can be written as the sum of two components $\mathbf{u} = \mathbf{u}_\parallel + \mathbf{u}_\perp$, where $\mathbf{u}_\perp = (\mathbf{u} \cdot \mathbf{e}_\perp)\mathbf{e}_\perp$ and $\mathbf{u}_\parallel = (\mathbf{u} \cdot \mathbf{e}_\parallel)\mathbf{e}_\parallel$ and $(\mathbf{e}_\parallel, \mathbf{e}_\perp)$ are unit vectors parallel and perpendicular to the swimmer. Here, we write explicit expressions of $\mathbf{u}_\parallel$ and $\mathbf{u}_\perp$ for each of the two arms forming the swimmer. For convenience, we denote the arm oriented at $-(\theta - \alpha)$ by arm 1 and that oriented at $\theta + \alpha$ by arm 2, see
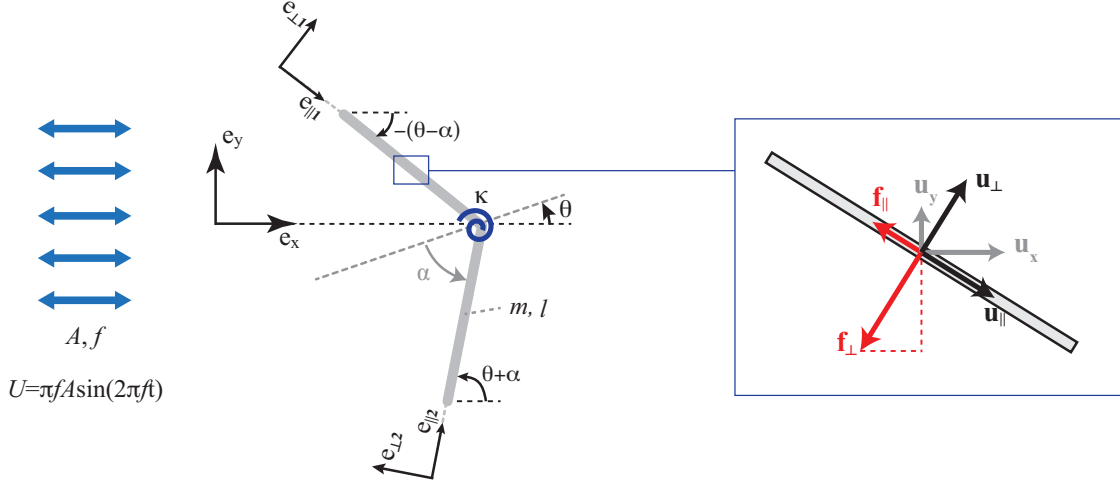
5

FIG. 1. Deformable swimmer consisting of two rigid bars of mass m and length l connected at one end via a torsional spring of stiffness κ in a zero-mean oscillatory background flow of amplitude A and frequency f. The hydrodynamic drag force acting on each segment of the body is calculated using the resistive force theory for slender filaments. The drag anisotropy provides a means to generate forces that are not necessarily aligned with the direction of actuation by the background flow (see text for notation).

Fig. 1(a). Consider an infinitesimal segment $\mathrm{d}s$ of arm 1 located at an arc-length s measured from the swimmer's apex. The local components of the translational velocity $\mathbf{u}_1(s,t)$ of arm 1 are given by

$$
\begin{aligned}
\mathbf{u}_{\perp 1} &= \left[-\dot{x}\sin(\theta-\alpha) + \dot{y}\cos(\theta-\alpha) - s(\dot{\theta}-\dot{\alpha}) \right]\mathbf{e}_{\perp 1}, \\
\mathbf{u}_{\|1} &= \left[\dot{x}\cos(\theta-\alpha) + \dot{y}\sin(\theta-\alpha) \right]\mathbf{e}_{\|1}.
\end{aligned}
\tag{2}
$$

Similar expressions can be readily obtained for the components of the local translational velocity $\mathbf{u}_2(s,t)$ of arm 2,

$$
\begin{aligned}
\mathbf{u}_{\perp 2} &= \left[-\dot{x}\sin(\theta+\alpha) + \dot{y}\cos(\theta+\alpha) - s(\dot{\theta}+\dot{\alpha}) \right]\mathbf{e}_{\perp 2}, \\
\mathbf{u}_{\|2} &= \left[\dot{x}\cos(\theta+\alpha) + \dot{y}\sin(\theta+\alpha) \right]\mathbf{e}_{\|2}.
\end{aligned}
\tag{3}
$$

The local directions $(\mathbf{e}_{\|1}, \mathbf{e}_{\perp 1})$ and $(\mathbf{e}_{\|2}, \mathbf{e}_{\perp 2})$ are indicated on Fig. 1.

  d. Hydrodynamic forces and moments. We compute the drag forces acting on the body using the resistive force theory for slender filaments. Accordingly, the local drag force $\mathbf{f_d}$ per unit length opposing the swimmer's motion relative to the background flow can be written as the sum of two components: a parallel component $\mathbf{f}_{\|} = -\xi_{\|}[\mathbf{u}_{\|} - U(\mathbf{e}_x \cdot \mathbf{e}_{\|})\mathbf{e}_{\|}]$

6

and a perpendicular component $\mathbf{f}_\perp = -\xi_\perp [\mathbf{u}_\perp - U(\mathbf{e}_x \cdot \mathbf{e}_\perp)\mathbf{e}_\perp]$ as depicted in Fig. 1. Here, $U = \pi A \sin(2\pi t)$ is the dimensionless flow velocity. The drag coefficients per unit length $\xi_\parallel$ and $\xi_\perp$ are proportional to the fluid viscosity and are set to $\xi_\parallel = \eta$ and $\xi_\perp/\xi_\parallel = 2$. This drag anisotropy ($\xi_\perp \neq \xi_\parallel$) is essential for locomotion in viscous flows; see, for example, [34] and references therein. Applying these expressions locally to bars 1 and 2, we get that $\mathbf{f}_{\mathbf{d}1} = \mathbf{f}_{\parallel 1} + \mathbf{f}_{\perp 1}$ and $\mathbf{f}_{\mathbf{d}2} = \mathbf{f}_{\parallel 2} + \mathbf{f}_{\perp 2}$, where

$$\mathbf{f}_{\parallel 1} = -\xi_\parallel \left[\mathbf{u}_{\parallel 1} - U \cos(\theta - \alpha)\mathbf{e}_{\parallel 1} \right], \qquad \mathbf{f}_{\perp 1} = -\xi_\perp \left[\mathbf{u}_{\perp 1} + U \sin(\theta - \alpha)\mathbf{e}_{\perp 1} \right], \qquad (4)$$

and

$$\mathbf{f}_{\parallel 2} = -\xi_\parallel \left[\mathbf{u}_{\parallel 2} - U \cos(\theta + \alpha)\mathbf{e}_{\parallel 2} \right], \qquad \mathbf{f}_{\perp 2} = -\xi_\perp \left[\mathbf{u}_{\perp 2} - U \sin(\theta + \alpha)\mathbf{e}_{\perp 2} \right]. \qquad (5)$$

The net hydrodynamic drag force on each arm is obtained by integrating the local drag force along the length of the arm. Namely, the net drag forces on arms 1 and 2 are given by $\mathbf{F}_1 = \int_0^l \mathbf{f}_{\mathbf{d}1} \, ds$ and $\mathbf{F}_2 = \int_0^l \mathbf{f}_{\mathbf{d}2} \, ds$. The net drag moments about the apex of the swimmer are given by $\mathbf{M}_1 = -\mathbf{e}_{\parallel 1} \times \int_0^l \mathbf{f}_{\perp 1} \, s \, ds$ and $\mathbf{M}_2 = -\mathbf{e}_{\parallel 2} \times \int_0^l \mathbf{f}_{\perp 2} \, s \, ds$.

To conclude, we note that the resistive force theory does not take into consideration hydrodynamic interactions between the segments of the swimmers, which may be relevant near the swimmer's apex, depending on the opening angle. A rough calculation of these hydrodynamic interactions show that they contribute only slightly to the overall drag forces and lead to qualitatively similar results [35].

e. *Equations of motion.* The equations governing the free motion of the swimmer in oscillatory background flows are obtained from the balance of linear and angular momenta of the system. To this end, we write the balance laws for each arm independently. We then add the balance of linear momenta for the two arms to obtain the translational equations of motion of the system. For convenience, we keep the rotational equations of motion in terms of $\theta - \alpha$ and $\theta + \alpha$ instead of rewriting them in terms of the shape angle α and orientation θ. To this end, we get

$$\mathbf{M}\ddot{\mathbf{q}} = \mathbf{F}_m + \mathbf{F}_k + \mathbf{F}_d, \qquad (6)$$

7

where $\mathbf{q} = [x, y, \theta - \alpha, \theta + \alpha]^T$, $()^T$ is the transpose operator, and $\ddot{()} = \partial^2/\partial t^2$ is the second time derivative. In (6), $\mathbf{M}$ is the mass matrix given by

$$\mathbf{M} = \begin{bmatrix} 2m & 0 & \frac{ml}{2}S_{\theta-\alpha} & \frac{ml}{2}S_{\theta+\alpha} \\ 0 & 2m & -\frac{ml}{2}C_{\theta-\alpha} & -\frac{ml}{2}C_{\theta+\alpha} \\ \frac{ml}{2}S_{\theta-\alpha} & -\frac{ml}{2}C_{\theta-\alpha} & \frac{ml^2}{3} & 0 \\ \frac{ml}{2}S_{\theta+\alpha} & -\frac{ml}{2}C_{\theta+\alpha} & 0 & \frac{ml^2}{3} \end{bmatrix}, \tag{7}$$

where we used the abbreviations $S_{\theta+\alpha} = \sin(\theta + \alpha)$, $S_{\theta-\alpha} = \sin(\theta - \alpha)$, $C_{\theta+\alpha} = \cos(\theta + \alpha)$, and $C_{\theta-\alpha} = \cos(\theta - \alpha)$. The terms $\mathbf{F}_m$, $\mathbf{F}_k$ and $\mathbf{F}_d$ on the right-hand side of (6) are the inertial, spring and hydrodynamic forces and moments, respectively. The inertial and spring forces and moments are given by

$$\mathbf{F}_m = \begin{bmatrix} -\frac{ml}{2}\left[C_{\theta-\alpha}(\dot{\theta} - \dot{\alpha})^2 + C_{\theta+\alpha}(\dot{\theta} + \dot{\alpha})^2\right] \\ -\frac{ml}{2}\left[S_{\theta-\alpha}(\dot{\theta} - \dot{\alpha})^2 + S_{\theta+\alpha}(\dot{\theta} + \dot{\alpha})^2\right] \\ 0 \\ 0 \end{bmatrix}, \quad \mathbf{F}_k = \begin{bmatrix} 0 \\ 0 \\ \kappa(\alpha - \alpha_r) \\ -\kappa(\alpha - \alpha_r) \end{bmatrix}, \tag{8}$$

where α_r is the rest angle of the torsional spring. The hydrodynamic forces and moments are given by

$$\mathbf{F}_d = \begin{bmatrix} C_{\theta-\alpha} & -S_{\theta-\alpha} & C_{\theta+\alpha} & S_{\theta+\alpha} \\ S_{\theta-\alpha} & C_{\theta-\alpha} & S_{\theta+\alpha} & -C_{\theta+\alpha} \\ 0 & -\frac{l}{2} & 0 & 0 \\ 0 & 0 & 0 & \frac{l}{2} \end{bmatrix} \begin{bmatrix} F_{\|1} \\ F_{\perp 1} \\ F_{\|2} \\ F_{\perp 2} \end{bmatrix}. \tag{9}$$

where $F_{\|1}$ and $F_{\perp 1}$ are the components of the net drag force $\mathbf{F}_1$ on arm 1,

$$F_{\perp 1} = -\xi_\perp l\left[-(\dot{x} - U)S_{\theta-\alpha} + \dot{y}C_{\theta-\alpha} - \frac{l}{2}(\dot{\theta} - \dot{\alpha})\right],$$
$$\tag{10}$$
$$F_{\|1} = -\xi_\| l\left[(\dot{x} - U)C_{\theta-\alpha} + \dot{y}S_{\theta-\alpha}\right].$$

and $F_{\|2}$ and $F_{\perp 2}$ are the components of $\mathbf{F}_2$ on arm 2,

$$F_{\perp 2} = -\xi_\perp l\left[(\dot{x} - U)S_{\theta+\alpha} - \dot{y}C_{\theta+\alpha} + \frac{l}{2}(\dot{\theta} + \dot{\alpha})\right],$$
$$\tag{11}$$
$$F_{\|2} = -\xi_\| l\left[(\dot{x} - U)C_{\theta+\alpha} + \dot{y}S_{\theta+\alpha}\right].$$

8

f. Massless swimmers. Consider the special case of zero mass $m = 0$ and finite spring stiffness κ. Equations (6) reduce to a set of first-order ordinary differential equations

$$\dot{x} = U, \quad \dot{y} = 0, \quad \dot{\theta} = 0, \quad \dot{\alpha} = -\frac{4\kappa}{3l^3\xi_\perp}(\alpha - \alpha_r). \tag{12}$$

This system of decoupled linear equations can be solved analytically. The body moves with the background flow in the x-direction, while its position in the y-direction and its orientation θ remain constant for all time. The shape variable α changes according to

$$\alpha = \alpha_r + (\alpha(0) - \alpha_r)e^{-\frac{4\kappa}{3l^3\xi_\perp}t}. \tag{13}$$

That is, α converges exponentially fast to the spring rest angle α_r as time t increases. For fixed l and $\xi_\perp$, the convergence rate is faster for larger values of κ, that is, for stiffer springs.

g. Rigid swimmers. For rigid dense swimmers ($\kappa = \infty$, $m > 0$), the opening angle α is fixed, say $\alpha = \alpha_r$, and $\dot{\alpha} = \ddot{\alpha} = 0$. The elastic terms vanish in equation (6) and the equations reduce to

$$\dot{x} = U, \quad \dot{y} = 0, \quad \ddot{\theta} = -\frac{3\xi_\perp l}{4m}\dot{\theta} - \frac{3\cos\alpha_r}{2l}\dot{U}\sin\theta. \tag{14}$$

Clearly, without elasticity, the equations for x and y decouple from the orientation equation. The body moves with the background flow in the x-direction and maintains its initial position in the y-direction similar to the case of massless swimmers. However, the dynamics of the orientation angle θ is governed by a nonlinear *parametrically-excited* equation, reminiscent to the damped Matthieu equation, see, e.g., [36–40]. The case $\theta(0) = 0$ is a fixed point of this equation. By analogy to the damped Matthieu equation, a detailed study of the stability of this fixed point should reveal transitions from stable and unstable behavior depending on parameter values. In this study, we focus on the stability of the system of equations (6) when both inertia and elasticity are at play, as discussed in section III.

h. Work and efficiency. We compute the average work W done by the hydrodynamic forces on the swimmer over one period T of background flow oscillations,

$$W = \frac{1}{T}\int_t^{t+T}\left[\int_0^l (\mathbf{f_{d1}} \cdot \mathbf{u_1} + \mathbf{f_{d2}} \cdot \mathbf{u_2})\ ds\right] dt. \tag{15}$$

The net displacement of the swimmer along the x-axis, if any, over one oscillation period of the background flow can be measured using the T-averaged quantity

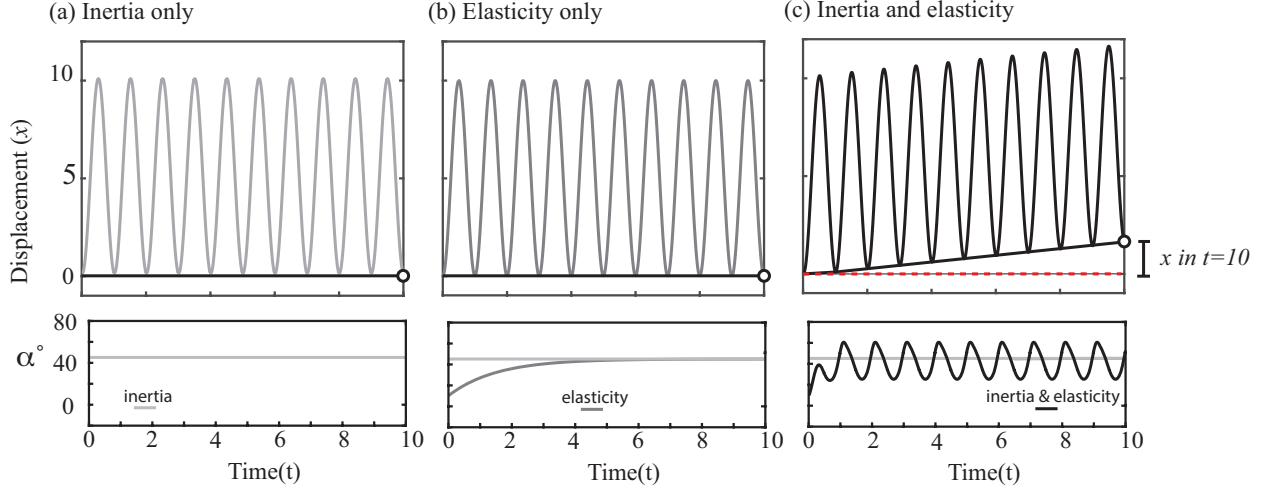$$\langle x \rangle = \frac{1}{T}\int_t^{t+T} x(t)dt. \tag{16}$$

9

FIG. 2. Displacement x shown in grey and time averaged displacement $\langle x \rangle$ shown in solid black (top row) and shape changes α versus time (bottom row) for: (a) rigid swimmer of mass $m = 1$ and infinite spring stiffness, (b) elastic swimmer of zero mass and spring stiffness $k = 50$, and (c) swimmer of mass $m = 1$ and spring stiffness $k = 50$. In all cases, the rest angle of the spring is $\alpha_r = 45°$, the fluid viscosity is $\eta = 50$ and the oscillatory background flow is given by $U = A\pi \sin(2\pi t)$ where $A = 10$. The initial conditions are $x(0) = \dot{x}(0) = 0$, $y(0) = \dot{y}(0) = 0$, $\theta(0) = \dot{\theta}(0) = 0$, $\alpha(0) = 10°$ and $\dot{\alpha}(0) = 0$.

For the cases where locomotion is achievable ($\langle x \rangle \neq 0$), we define the cost of locomotion c as the average work divided by the average distance over one period,

$$c = \frac{W}{\langle x \rangle}. \tag{17}$$

Smaller c means less work "used" for a fixed distance traveled. It is convenient to denote the efficiency of the system e as the inverse of the cost of locomotion, $e = 1/c$. This definition of efficiency is consistent with the one used in [41] and [42] for underwater and terrestrial locomotion. Intuitively, e is analogous to the "miles-per-gallon" concept.

III. RESULTS

We first examine the behavior of the swimmer when placed in a symmetric configuration about the x-axis. We solve (6) numerically for initial conditions $x(0) = \dot{x}(0) = 0$, $y(0) = \dot{y}(0) = 0$, $\theta(0) = \dot{\theta}(0) = 0$, $\alpha(0) = 10°$ and $\dot{\alpha}(0) = 0$. Fig. 2 depicts the displacement x versus time t for three distinct swimmers: (a) a rigid swimmer of mass $m = 1$ and infinite
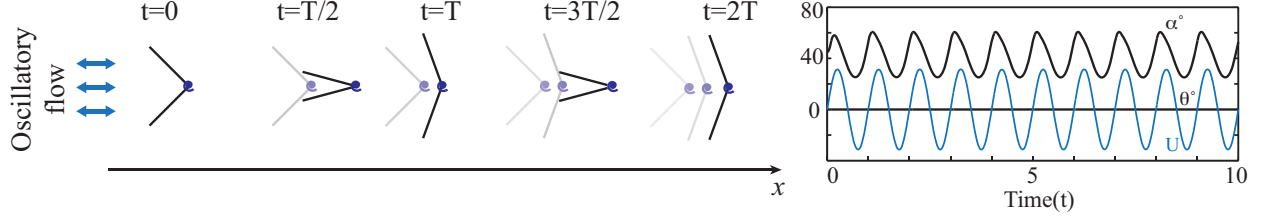
10

FIG. 3. The swimmer shown in Fig. 2(c) changes shape passively and swims parallel to the flow. The opening angle α oscillates at the same frequency as the background oscillatory flow while the orientation θ of the swimmer is identically zero.

spring stiffness κ, (b) an elastic massless swimmer with $m = 0$ and finite $\kappa = 50$, and (c) a swimmer of finite mass $m = 1$ and spring stiffness $\kappa = 50$. In all three cases, the remaining parameter values are set to $\alpha_r = 45°, \eta = 50$ and $A = 10$. The rigid swimmer and the elastic massless swimmer exhibit oscillatory motion but no net displacement in oscillatory flows, as predicted by (12) and (14). This zero net motion is consistent with Purcell's scallop theorem, where two-link bodies connected via one hinge cannot swim by reciprocal motions in drag-dominant flows. However, the swimmer with finite mass and elasticity swims parallel to the flow oscillations, with net displacement $\langle x \rangle = \frac{1}{T} \left(\int_t^{t+T} x(t) dt \right)$ per oscillation period T, see Fig. 2(c). This is because inertia (non-zero mass) introduces a nonlinearity in the forces $\mathbf{F}_m$ that couples the displacement $x(t)$ to the shape deformations $\alpha(t)$ due to the finite spring stiffness, and leads to breaking the time-reversible symmetry of two-link swimmers in drag-dominant flows. The opening angle α of the rigid swimmer is constant while that of the massless swimmer converges exponentially to the rest angle of the spring $\alpha_r = 45°$, consistent with (13). When inertia and elasticity are combined, the swimmer undergoes periodic closing and opening motions at the same frequency as that of the background flow U, as illustrated in Fig. 3. In all three cases, the displacement in the y direction and the orientation θ are identically zero owing to the symmetry of the problem and initial conditions.

Fig. 4 (top row) shows the net displacement $\langle x \rangle$ of the swimmer as a function of the four dimensionless parameters m, κ, A and η. In all simulations, initial conditions are set to $\theta(0) = \dot{\theta}(0) = 0$ and $\alpha(0) - \alpha_r = \dot{\alpha}(0) = 0$ and the rest angle of the spring is set to $\alpha_r = 45°$. The swimmer's mass m affects the amount and direction of net displacement (Fig. 4(a)). For $m \approx 5$, the swimmer achieves maximum displacement in the positive x-
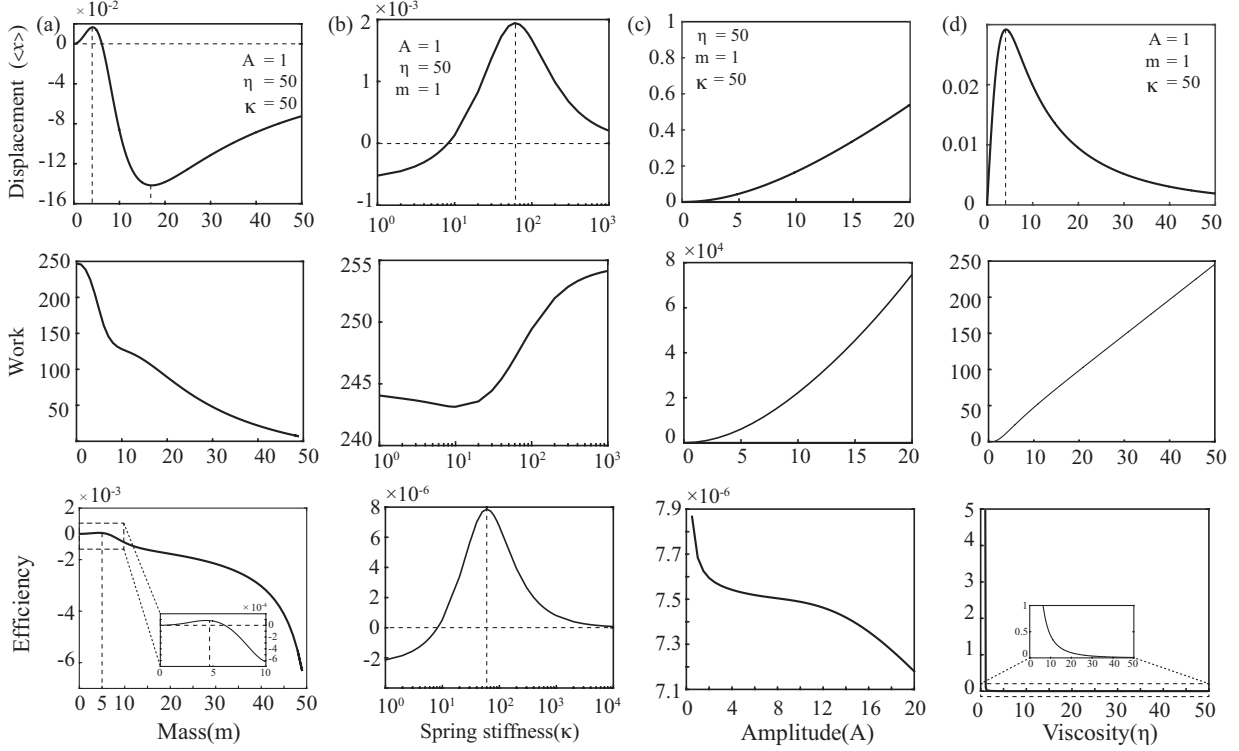
11

FIG. 4. Net displacement, work and efficiency in symmetric motions as a function of (a) mass m, (b) spring stiffness κ, (c) amplitude A and (d) viscosity η. The nominal parameters are set as $m = 1$, $\kappa = 50$, $A = 1$ and $\eta = 50$.

direction, whereas $m \approx 17$ produces maximum negative displacement. The displacement converges to zero for massive swimmers (as $m \to \infty$), consistent with physical intuition. The spring stiffness κ also affects the amount and direction of net displacement (Fig. 4(b)). Maximum displacement is achieved in the positive x-direction at $\kappa \approx 60$. The displacement tends to zero as $k \to \infty$, that is, as the swimmer approaches a rigid body. The effects of the amplitude of flow oscillations A and fluid viscosity η on the displacement are shown in Fig. 4(c) and (d). The displacement grows monotonically with increasing A. The net displacement goes to zero as $\eta \to 0$ because the hydrodynamic drag forces are proportional to viscosity and approach zero as $\eta \to 0$. In this limit, the assumption of drag-dominant flows breaks down and fluid inertia should be explicitly accounted for in the model, which is beyond the scope of the present study. As $\eta \to \infty$, the drag forces go to infinity and overpower the interplay between inertia and elasticity of the swimmer. No net displacement is achievable in this limit. Displacement is maximum at $\eta \approx 5$.
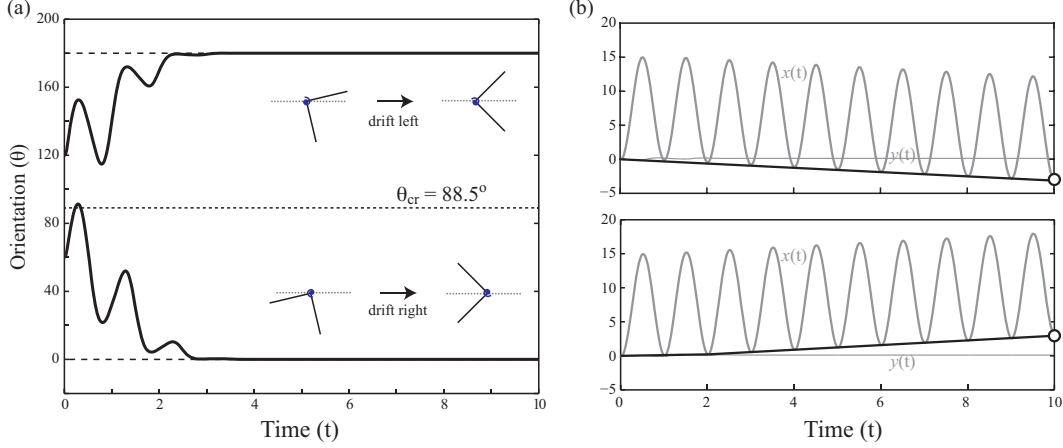
12

FIG. 5. Linear motion of a symmetric swimmer. (a) Time courses of orientation θ subject to two initial perturbations $\theta(0) = 60°$ and $120°$. Initially, $\alpha(0) = \alpha_r = 45°$. And the critical perturbation $\theta_{cr} = 88.5°$ with parameter values given as $m = 1$, $\kappa = 50$, $A = 15$, and $\eta = 50$. (b) Time evolution of the swimmer position $(x(t), y(t))$. The smaller perturbation $\theta(0) = 60° < \theta_{cr}$ results in a positive net displacement in the x-direction, shown in the bottom figure. And the larger $\theta(0)$ causes the swimmer to flip its direction.

The hydrodynamic work W done by the fluid on the passive swimmer depends non-monotonically on the swimmer's properties m and k but increases monotonically with increasing flow amplitude A and viscosity η, as shown in Fig. 4 (middle row). Correspondingly, the efficiency e is optimal for finite values of $m_{\text{op}} = 5$ and $k_{\text{op}} = 60$, as depicted in Fig. 4 (bottom row). Small m leads to weaker symmetry-breaking and propulsion, whereas large m requires more effort to displace the swimmer by a given distance. Similar argument holds for the effect of spring stiffness: elasticity is weaker for $\kappa < \kappa_{\text{op}}$ leading to weaker elastic energy storage and breaking of the time reversal symmetry whereas $\kappa > \kappa_{\text{op}}$ indicates stiffer springs that require more work to be actuated, resulting in smaller efficiencies.

We now examine the stability of the passive motion in the x-direction when the swimmer is subject to perturbations in its initial orientation $\theta(0)$. More specifically, we keep the same initial condition for the opening angle $\alpha(0) = \alpha_r = 45°$ but perturb the orientation angle $\theta(0)$ from 0 to $180°$ by increments of $1°$. We numerically integrate the nonlinear system of equations (6) from $t = 0$ to $t = 200$ using the adaptive fourth- and fifth-order Runge Kutta scheme in Matlab. We find that for initial perturbations below a critical value θ_{cr}, the swimmer's orientation converges to $\theta = 0$ and the swimmer continues to move in the
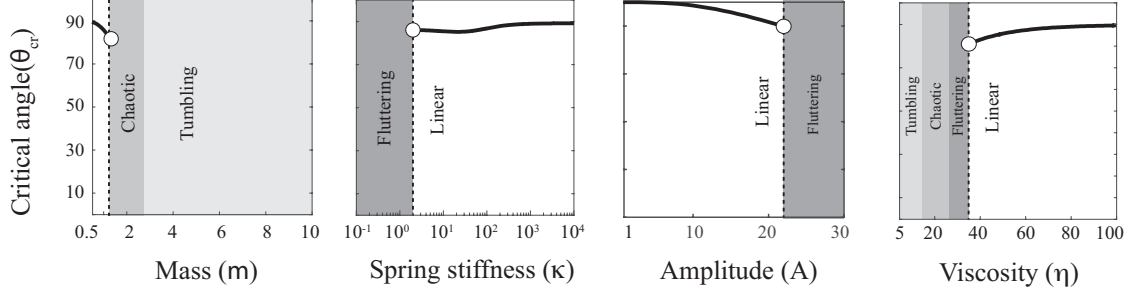
13

FIG. 6. Dynamics behavior of the swimmer as a function of mass, spring stiffness, amplitude and viscosity. Nominal parameter values are chosen as $m = 1$, $\kappa = 50$, $A = 15$, and $\eta = 50$.

positive x-direction, whereas for perturbations larger than θ_{cr}, the swimmer's orientation flips to $\theta = 180°$ and the swimmer changes its direction of motion. Fig. 5(a) shows the time evolution of the orientation θ subject to two initial perturbations $\theta(0) = 60°$ and $\theta(0) = 120°$. Here, parameter values are set to $m = 1$, $\kappa = 50$, $\eta = 50$ and $A = 15$. The critical orientation θ_{cr} across which the swimmer flips its direction of motion is 88.5°. For $\theta(0) = 60° < \theta_{cr}$, the swimmer aligns itself with the background flow and moves to the right and for $\theta(0) = 120° > \theta_{cr}$, the swimmer also aligns with the oscillatory flow but flips its orientation and drifts to the left.

A close examination of the dependence of θ_{cr} on the mass m and spring stiffness κ of the swimmer and the amplitude A and viscosity η of the background flow shows that the value of θ_{cr} is not very sensitive to these parameters; see the thick black lines in Fig. 6 delineating the boundary between the basins of attraction of $\theta = 0$ and $\theta = 180°$. This parametric study also reveals that the swimmer's motion depends non-trivially on parameter values. More specifically, we find that symmetric swimming in the x-direction (with $\theta = 0$ or $\theta = 180°$) is not always a stable attracting behavior. The grey regions in Fig. 6 highlight the parameter values for which such symmetric swimming is unstable. In these regions, the passive two-link swimmer follows one of three distinct behaviors: fluttering, chaotic or tumbling. Fig. 7 shows representative trajectories of all four types of behavior: (a) stable symmetric swimming in the x-direction, which we denote as "linear" swimming, (b) fluttering motion where the swimmer advances along the x-direction while periodically moving from side-to-side in the y-direction, (c) chaotic-like motion, and (d) tumbling motion where the swimmer's apex periodically traces a closed trajectory while θ increases monotonically.

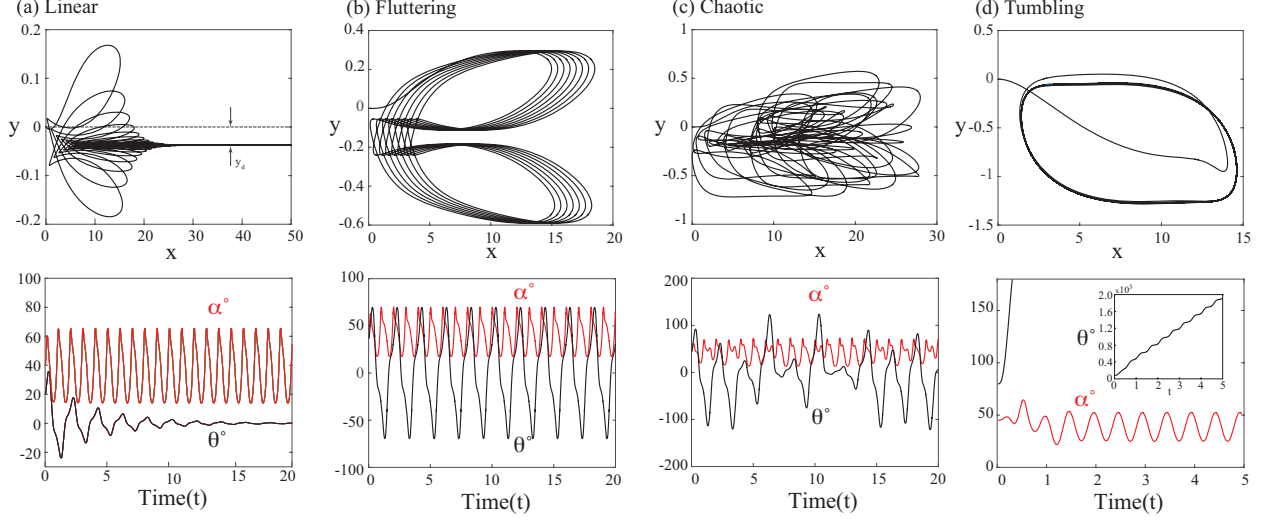We analyze the passive stability of symmetric swimming by imposing a finite initial per-

FIG. 7. Behaviors of the swimmer: (a) Linear swimming in the x-direction for $\eta = 40$, $\theta(0) = 30°$ and $\alpha(0) = 40°$. (b) Fluttering from side to side for $\eta = 40$, $\theta(0) = 30°$ and $\alpha(0) = 40°$. (c) Chaotic-like motion for $\eta = 25$, $\theta(0) = 45°$ and $\alpha(0) = 45°$. (d) Tumbling behavior for $\eta = 6$, $\theta(0) = 80.6°$ and $\alpha(0) = 45°$. All other parameters have the same nominal values as in Fig. 6.
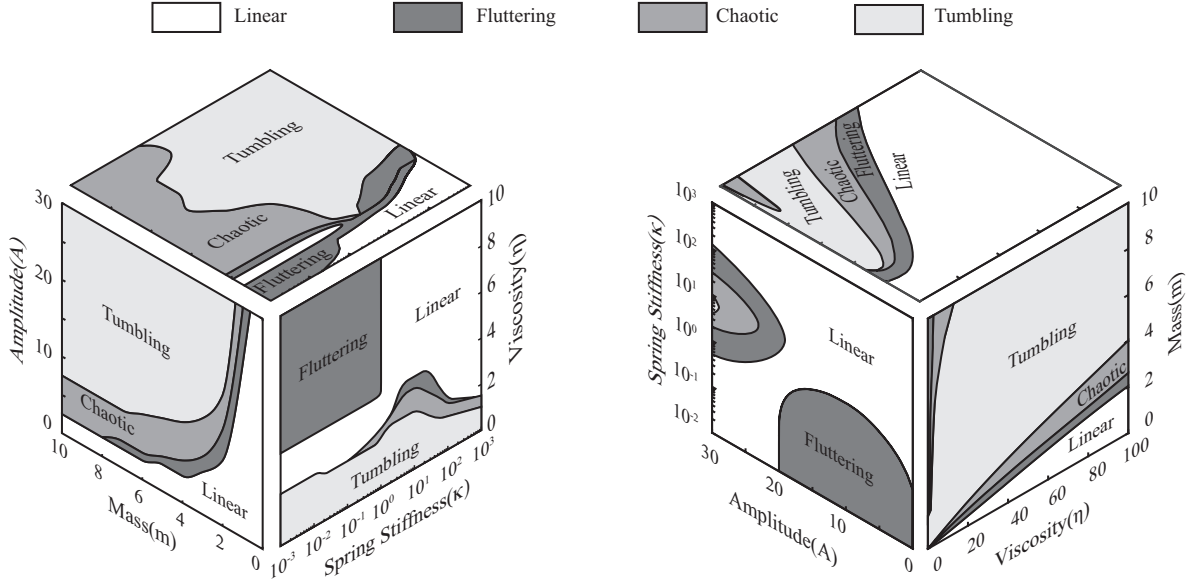

FIG. 8. Behavior of symmetric swimming mapped onto the parameter spaces. Linear, fluttering, chaotic and tumbling. The cross-sections correspond to nominal values of the four dimensionless parameters, which we set to $m = 1$, $\kappa = 50$, $A = 15$ and $\eta = 50$. Initial conditions are $\alpha(0) = \alpha_r = 45°$ and are subject to different initial orientations $\theta(0)$.

turbation $\theta(0)$ and solving the fully nonlinear governing equations of motion in (6). We focus

15

on the time evolution of the orientation angle θ: if it oscillates with decreasing amplitude and converges to $\theta = 0$, we say linear swimming in the x-direction is passively stable. Otherwise, linear swimming is unstable. We then classify the type of behavior in the unstable regions of the parameter space into fluttering, chaotic-like, and tumbling. We map out these results to six distinct cross-sections of the four-dimensional parameter space (m, κ, A, η) as shown in Fig. 8. Here, each cross-section is discretized using an adaptive mesh of increments Δm, $\Delta \eta$, ΔA, $\Delta(\log \kappa)$ varying in size from 0.25 to 1. The simulations at each point in the parameter space are repeated for several values of the initial perturbation $\theta(0)$ to ensure that the results are independent of the size of the initial perturbation and reflect the intrinsic behavior of the system. We obtain clear transitions from stable (white regions) to unstable (grey regions) linear swimming. For example, in the (A, η) cross-section, we see that symmetric swimming is stable when the oscillation amplitude A is small and fluid viscosity η is large. The (m, κ) cross-section reveals that if the spring is too "floppy," the motion is more likely to be unstable. Larger mass m is also associated with unstable linear swimming. In the regions where linear swimming is unstable, we observe ordered transitions from linear to fluttering, chaotic then tumbling motions. Similar transitions have been reported in the problem of coins and flat plates falling in water [43–46] at intermediate and large Re. The wake of the falling object plays an important role in these transitions; see, e.g., [47] and references therein. Here, transitions between these regimes occur at zero Re as a result of the interplay between the swimmer's properties (m and κ) and the fluid properties (A and η). To our best knowledge, this is the first time such detailed parametric study is conducted and such transitions are reported at zero Re. These transitions could have important implications on applications such as sorting of deformable cells and microstructures in microfluidic channels as well as on shedding light on the physical mechanisms underlying active and passive transitions in the behavior of microswimmers, as discussed next.

IV. DISCUSSION

We presented a novel mechanism for flow-driven locomotion of a Λ-shaped microswimmer. Namely, we examined the response of a deformable two-link swimmer in viscous fluid to background flow oscillations with zero mean velocity. We found that buoyant swimmers (or swimmers of negligible mass) as well as rigid swimmers exhibit no net displacement, con-

16

sistent with Purcell's scallop theorem. However, dense and simultaneously elastic swimmers are able to swim passively in oscillatory homogeneous flows along the flow lines, because the deformation of the Λ-shaped particle is different during the two half periods. Therefore the time-symmetry is broken and Purcell's scallop theorem does not apply.

For given flow parameters, the direction of motion (left or right) is dictated by the swimmer's properties, mass and spring stiffness, as well as by its initial orientation and spring rest angle. We then analyzed in details the effects of parameter values on the net displacement. We found that the net displacement increases monotonically with the oscillation amplitude. We also found that the swimming efficiency decreases monotonically with the amplitude and viscosity of the background flow while the mass and stiffness of the swimmer can be tuned to achieve optimal symmetric swimming. We then analyzed the stability of symmetric swimming when subject to perturbations in its initial orientation relative to the background flow oscillations. We found that, for a range of parameter values, symmetric swimming is a stable attracting solution. In fact, for these parameter values, we identified two stable orientations $\theta = 0$ and $\theta = 180°$ associated with two directions of motion of the swimmer: swimming to the right or to the left parallel to the oscillatory background flow. We probed the stability of these swimming motions by conducting a detailed parametric study. Our results show that, to achieve a stable motion by tuning the amplitude of the background flow oscillations, the swimmer should have small mass and large spring stiffness and should be swimming in a fluid of high viscosity, consistent with physical intuition. We also identified ranges of parameter values where these symmetric solutions are unstable and where the swimmer undergoes either fluttering, chaotic-like or tumbling behavior. These transitions could be exploited to design microfluidic channels for cell sorting by flow oscillations, where cells of different mass and elastic properties would respond differently to the same flow oscillations. Further, these transitions could provide physical mechanisms by which swimmers can be made to change their behavior passively from linear swimming to tumbling by tuning the flow properties.

The results presented will be modified, but qualitatively similar, when gravitational effects or hydrodynamic interactions between the arms are taken into account [35]. Our results are specific to passive swimming in oscillatory flows, with no direct control of the shape variable. However, an analogy can be made to active swimming where the swimmer's shape is actuated via internal forces or torques generated by the swimmer [48], as opposed to direct control

of the shape kinematics [1, 8–10]. Controlling the swimmer's forces or torques instead of its shape kinematics poses a problem of dynamic stability of motion similar to the stability problem considered here. Numerical evidence suggests that torque actuation of Purcell's three-link swimmer could lead to chaotic-like motion as well as stable swimming behavior depending on the actuation parameters [48]. This analogy motivates the following questions: would a detailed parametric study of the torque-actuated three-link swimmer in [48] reveal similar transitions from stable swimming to fluttering, chaotic-like and tumbling behavior? if so, could these transitions be related to the physical mechanisms that underly the transition from run to tumble in bacterial cells [4]? These questions will be addressed in future studies.

CONFLICT OF INTEREST STATEMENT

The authors declare that they have no conflict of interest.

---

[1] E. M. Purcell, Am. J. Phys **45**, 3 (1977).

[2] H. C. Berg, Biochemistry **72**, 19 (2003).

[3] H. C. Berg, Physics Today **5**, 53 (2005).

[4] H. C. Berg, *E. coli in Motion* (Springer Science & Business Media, 2008).

[5] C. Eloy and E. Lauga, Phys. Rev. Lett. **109**, 038101 (2012).

[6] H. Guo, J. Nawroth, Y. Ding, and E. Kanso, Phys. Fluids **26**, 091901 (2014).

[7] H. Guo and E. Kanso, Phys. Rev. E **93**, 033119 (2016).

[8] D. Tam and A. E. Hosoi, Phys. Rev. Lett. **98**, 068105 (2007).

[9] A. Najafi and R. Golestanian, Phys. Rev. E **69**, 062901 (2004).

[10] J. Avron, O. Gat, and O. Kenneth, Phys. Rev. Lett. **93**, 186001 (2004).

[11] S. Y. Tony, E. Lauga, and A. Hosoi, Phys. Fluids **18**, 091701 (2006).

[12] E. Passov and Y. Or, Eur. Phys. J. E **35**, 1 (2012).

[13] H. C. Fu, T. R. Powers, and C. W. Wolgemuth, Phys. Rev. Lett. **99**, 258101 (2007).

[14] D. Gonzalez-Rodriguez and E. Lauga, J. Phys. Condens. Matter **21**, 204103 (2009).

[15] L. Burton, R. L. Hatton, H. Choset, and A. Hosoi, Phys. Fluids **22**, 091703 (2010).

[16] T. Ishikawa and V. Vladimirov, J. Fluid Eng. **137**, 084501 (2015).

[17] I. Jo, Y. Huang, and E. Kanso, in *IEEE Conf. Decis. Control* (IEEE, 2016) p. In publish.

[18] B. J. Nelson, I. K. Kaliakatsos, and J. J. Abbott, Annu. Rev. Biomed. Eng. **12**, 55 (2010).

[19] H. Andersson and A. Van den Berg, Sensor Actuat. B-Chem. **92**, 315 (2003).

[20] C. W. Shields IV, C. D. Reyes, and G. P. López, Lab on a Chip **15**, 1230 (2015).

[21] M. Sitti, Nature **458**, 1121 (2009).

[22] R. Dreyfus, J. Baudry, M. L. Roper, M. Fermigier, H. A. Stone, and J. Bibette, Nature **437**, 862 (2005).

[23] U. K. Cheang, D. Roy, J. H. Lee, and M. J. Kim, Appl. Phys. Lett. **97**, 213704 (2010).

[24] A. Snezhko and I. S. Aranson, Nat. Mater. **10**, 698 (2011).

[25] S. T. Chang, V. N. Paunov, D. N. Petsev, and O. D. Velev, Nat. Mater. **6**, 235 (2007).

[26] G. Loget and A. Kuhn, Nat. Commun. **2**, 535 (2011).

[27] H.-R. Jiang, N. Yoshinaga, and M. Sano, Phys. Rev. Lett. **105**, 268302 (2010).

[28] S. Thutupalli, R. Seemann, and S. Herminghaus, New J. Phys. **13**, 073021 (2011).

[29] M. Leoni, J. Kotar, B. Bassetti, P. Cicuta, and M. C. Lagomarsino, Soft Matter **5**, 472 (2009).

[30] D. Klotsa, K. A. Baldwin, R. J. Hill, R. Bowley, and M. R. Swift, Phys. Rev. Lett. **115**, 248102 (2015).

[31] L. G. Leal, Ann. Rev. Fluid Mech. **12**, 435 (1980).

[32] B. Kaoui, Phys. Rev. E **77**, 021903 (2008).

[33] S. K. Doddi and P. Bagchi, Int. J. Multiphas. Flow **34**, 966 (2008).

[34] E. Lauga and T. R. Powers, Rep. Prog. Phys. **72**, 096601 (2009).

[35] M. Laumann, E. Kanso, D. Kienle, and W. Zimmermann, in preparation (2016).

[36] R. S. Zounes and R. H. Rand, Int. J. Nonlinear Mech. **37**, 43 (2002).

[37] R. S. Zounes and R. H. Rand, Nonlinear Dyn. **27**, 87 (2002).

[38] L. Ng and R. Rand, Chaos, Solitons & Fractals **14**, 173 (2002).

[39] E. Kanso, A. J. Szeri, and A. P. Pisano, J. Microelectromech. S. **13**, 323 (2004).

[40] R. Rand and T. Morrison, Nonlinear Dyn. **40**, 195 (2005).

[41] F. Jing and E. Kanso, Regul. Chaotic Dyn. **18**, 380 (2013).

[42] F. Jing and S. Alben, Phys. Rev. E **87**, 022711 (2013).

[43] S. B. Field, M. Klaus, M. Moore, and F. Nori, Nature **388**, 252 (1997).

[44] A. Andersen, U. Pesavento, and Z. J. Wang, J. Fluid Mech. **541**, 65 (2005).

[45] E. Kanso, L. Heisinger, and P. Newton, J. Fluid Mech. **742**, 243 (2014).

[46] P. Ern, F. Risso, D. Fabre, and J. Magnaudet, Annu. Rev. Fluid Mech. **44**, 97 (2012).

[47] L. Vincent, W. S. Shambaugh, and E. Kanso, J. Fluid Mech. **801**, 250 (2016).

[48] Y. Or, Phys. Rev. Lett. **108**, 258101 (2012).